International Journal of Applied Pharmaceutics

ISSN- 0975-7058 Vol 13, Issue 3, 2021

Original Article

BOOSTING THE SKIN DELIVERY OF CURCUMIN THROUGH STEARIC ACID-ETHYL CELLULOSE BLEND HYBRID NANOCARRIERS-BASED APPROACH FOR MITIGATING PSORIASIS

PANKAJ KUMAR JAISWAL, SANJOY DAS, MALAY K. DAS*

Drug Delivery Research Laboratory, Department of Pharmaceutical Sciences, Dibrugarh University, Dibrugarh, Assam 786004, India
***Email: mkdps@dibru.ac.in**

Received: 31 Dec 2020, Revised and Accepted: 09 Mar 2021

ABSTRACT

Objective: Curcumin presents poor topical bioavailability when administered orally, which poses a major hurdle in its use as an effective therapy for the management of psoriasis. The present study reports the utilization of lipid-polymer hybrid nanoparticles (LPHNPs) for the topical delivery of curcumin which can be a potential approach for mitigating psoriasis.

Methods: Curcumin-loaded LPHNPs were prepared by the emulsification solvent evaporation method and characterized. The optimized Curcumin-loaded LPHNPs (DLN-3) were further incorporated into 2% Carbopol 940 gels and evaluated for its therapeutic efficacy in the Imiquimod (IMQ)-induced psoriasis rat model.

Results: The average particle size, polydispersity index, zeta potential, drug entrapment and loading efficiency for DLN-3 were found to be 200.9 nm, 0.342,-28.3 mV, 87.40±0.99% and 4.57±0.04%, respectively. FT-IR, DSC and XRD studies confirmed that all the components used for the formulation are compatible with each other, whereas SEM and TEM analysis affirmed the spherical shape of LPHNPs with a smooth surface. The *in vitro* drug release studies suggest that curcumin was released from the LPHNPs in a sustained manner over a period of 24 h via super case II transport mechanism. Results of *in vitro* skin permeation study revealed that 38.39±2.67% of curcumin permeated at 12 h across excised pig ear skin with a permeation flux of 18.74±3.59 µg/cm^2/h. Further, *in vivo* evaluation and histopathological studies demonstrated that NLHG-1 hydrogels showed better therapeutic efficacy against the psoriatic skin lesions than the standard marketed gels.

Conclusion: These results suggest that the developed LPHNPs have a superior ability to improve the skin penetration or accumulation of DLN-3 within psoriatic skin and offer a potential delivery system for the management of psoriasis.

Keywords: Lipid-polymer hybrid nanoparticles, Curcumin, Topical gels, Psoriasis, Imiquimod

DOI: https://dx.doi.org/10.22159/ijap.2021v13i3.40668. Journal homepage: https://innovareacademics.in/journals/index.php/ijap

INTRODUCTION

Psoriasis is a consistently recurring, autoimmune, chronic inflammatory disorder of the skin that is estimated to affect approximately 2-4% of the population in Western countries and shows lower prevalence in Asian as well as African countries [1, 2]. The main pathological features of psoriasis are multifactorial, usually involving hyperplasia of the epidermis, abnormal genetic association and dysregulated signal processing of T cells as well as an imbalance between inflammatory mediators that promote the infiltration of leukocytes [3, 4]. Though major problems associated with psoriasis are relapsing and spontaneous remission, which may trigger by genetic, environmental and several other factors [5]. As there is no complete resolution for psoriasis to date, a stepwise strategy to healing is often employed with the initial use of topical treatment, act to phototherapy and pharmacotherapy. However, the presence of multilayered epidermal barriers of psoriatic skin causes hindrance to the entry of drug molecules to the inflamed site, resulting in the formation of severe adverse effects [6, 7]. To get better therapeutic benefits, several nanoparticles have been widely explored for topical drug delivery, including polymeric, lipid, metallic, carbon-based and vesicular nanoparticles. These nanoparticles are shown to be promising in dermatological disease management by boosting drug solubility and bioavailability of poorly water-soluble drugs [8-13].

Nevertheless, single nanoparticles unable to provide these benefits at a time and have some common limitations in terms of rapid drug diffusion, instability during storage and uncontrolled drug release [14-16]. Recently, lipid-polymer hybrid nanoparticles (LPHNPs) have gained much attention as their outstanding benefits to resolve these problems. This system can take the functions of the lipid and polymeric nanoparticles, which comprises two distinct components i.e., an innermost hydrophobic polymeric core which encapsulating the poorly water-soluble drugs and an outermost lipid layer that act as a molecular fence to promote drug retention inside the polymeric core. Although for topical application, these hybrid nanoparticles have been incorporated into hydrogels, which makes the formulation very pertinent to achieving the desired effect [17, 18].

Curcumin is a yellow-colored polyphenolic compound obtained from the rhizome of the perennial herb *Curcuma longa* and possesses outstanding anticancer properties [19]. Despite the promising therapeutic value offered by curcumin, its translation from basic research to clinical application is limited due to poor water solubility and low bioavailability [20, 21]. Therefore, the present study was engineered to develop and characterize the LPHNP based hydrogels for the topical delivery of curcumin and compares the *in vivo* anti-psoriatic efficacy with the commercial marketed product in hopes of assessing a relatively effective and safe medicine for the psoriasis treatment.

MATERIALS AND METHODS

Materials

Curcumin and stearic acid were purchased from Hi-Media Laboratories Pvt. Ltd., Mumbai, India. Ethylcellulose was purchased from Loba Chemie Pvt. Ltd., Mumbai, India. Polyethylene glycol 400 and tween 80 were purchased from Sisco Research Laboratories Pvt. Ltd., Mumbai, India. Carbopol 934, ethanol and triethanolamine were purchased from Research Lab Fine Chem Industries, Mumbai, India. All other reagents and chemicals used were of analytical grade.

Preparation of lipid-polymer hybrid nanoparticles (LPHNPs)

The LPHNPs were prepared by the emulsification solvent evaporation method with slight modifications [22, 23]. Briefly, stearic acid and ethyl cellulose were dissolved in 2 ml of ethanol in a beaker and curcumin was added into the lipid-polymer (oil) phase. Resulting lipid-polymer (oil) phase was added dropwise into 10 ml of aqueous phase (1% w/v Tween 80) under continuous stirring at 15000 rpm for 5 min using a homogenizer (Ultra-Turrax T 25

Digital, IKA Germany) and further subjected to sonication at 50-55 °C using bath sonicator (UCB 30, Spectralab Instruments, India) for 20 min to agitate particles and collapse air bubbles in the liquid medium. The dispersion was then stirred continuously for complete evaporation of the organic solvent. Spontaneously, the lipid layer was self-assembled around the polymeric core resulting in the formation of LPHNPs. The nanoparticle dispersions were centrifuged at 10000 rpm for 15 min. The supernatant were discarded and the solid mass was washed three times with distilled water. Finally, the developed formulations were freeze-dried (temperature-80 °C and pressure 0.02 mbar) using lyophilizer (SS1-LYO, Southern Scientific Lab Instruments, India) with 5% mannitol for cryoprotection and stored in an airtight container for further use. The blank formulations were prepared without the addition of drugs using the same procedure.

Characterization of LPHNPs

Particle size, polydispersity index and zeta potential

The average particle size and polydispersity index of the prepared LPHNPs were measured by Dynamic Light Scattering using the particle size analyzer (90 Plus, Brookhaven Instruments, USA). The zeta potential of the prepared LPHNPs was measured by Zetasizer (Nano ZS, Malvern Instruments, UK) to assess the surface charge. In every cases, the freeze-dried LPHNPs were dispersed in distilled water (0.1% w/v) and subsequently analyzed [24].

Drug entrapment and drug loading efficiency

The drug entrapment and drug loading efficiency of the prepared LPHNPs were determined by measuring the concentration of free drug in the supernatant when it exposed to high-speed centrifugation. Simply, the prepared LPHNPs were subjected to centrifugation (R 8C DX, REMI, India) at 12500 rpm for 30 min to get the clear supernatant. The supernatant was then diluted with ethanol and the concentration of free drug present in the supernatant was determined spectrophotometrically at 426 nm using UV-Visible Spectrophotometer (UV 1800, Shimadzu, Japan) with respect to blank ethanol. The percentage drug entrapment and loading efficiency were determined according to the following formulas [25].

$$\% \text{ Drug Entrapment Efficiency} = \frac{\text{Total Drug} - \text{Free Drug}}{\text{Total Drug}} \times 100$$

$$\% \text{ Drug Loading Efficiency} = \frac{\text{Total Drug} - \text{Free Drug}}{\text{Total Weight of Nanoparticles}} \times 100$$

Drug-excipient compatibility studies

To estimate any type of interaction between the drug and excipients, FT-IR, DSC and XRD analysis was done for the drug, polymer, lipid, physical mixture and drug-loaded LPHNPs.

In the FT-IR analysis, pure drug curcumin, ethylcellulose, stearic acid, physical mixture and blank LPHNPs and curcumin-loaded LPHNPs were placed on the sample holder of the FT-IR spectrometer (Alpha, Bruker, Germany). The FT-IR spectrum was obtained by scanning in the wavenumber region of 4000-400 cm^{-1} to record characteristics peaks and functional groups of the above samples [26].

In the DSC analysis, pure drug curcumin, ethylcellulose, stearic acid, physical mixture and blank LPHNPs and curcumin-loaded LPHNPs were crimped in standard aluminum pans of the Differential Scanning Colorimeter (DSC 4000, Perkin Elmer, USA) and heated from 0 to 400 °C at a heating rate of 10 °C per minutes under constant purging of dry nitrogen. The DSC analysis was mainly performed to investigate the thermal behavior of the various samples [27].

In the XRD analysis, the diffraction patterns of pure drug curcumin, ethylcellulose, stearic acid, physical mixture and blank LPHNPs and curcumin-loaded LPHNPs were recorded by X-Ray Diffractometer (Ultima IV, Rigaku, Japan) using Cu anode at a voltage of 40 kV and a current of 30 mA. The samples were scanned in the range of 10-80 ° diffraction angle with a speed of 2 ° per minute. XRD analysis was carried out to know the crystalline structure of the above samples [28].

Morphological studies

The external and internal structure of the prepared LPHNPs was examined by scanning electron microscopy (SEM) and transmission electron microscopy (TEM).

For SEM analysis, the LPHNPs were dispersed in distilled water and a drop of solution was placed on metal stubs with double adhesive carbon-coated tape. The metal stubs were then coated with a layer of gold to minimize the surface charging. The coated samples were randomly scanned by scanning electron microscope (MultiSEM 505, ZEISS, Germany) at an accelerating voltage of 20 kV and photographs with various magnifications were captured into a computer [29].

For TEM analysis, the LPHNPs were dispersed in distilled water and a drop of sample solution was placed on the carbon-coated copper grid. The grid surface was properly air dried before loaded into the specimen holder. The samples were then subsequently scanned by transmission electron microscope (JEM 2100, JEOL, USA) operating at an accelerating voltage of 200 kV and photographs were captured using an advanced CCD camera [30].

***In vitro* drug release studies**

The *in vitro* drug release study was performed using the dialysis bag method to determine the release of curcumin from LPHNPs. Initially, the dialysis membrane having a molecular weight cutoff 12000 Da, soaked in distilled water and subsequently filled with 2 ml of LPHNPs dispersion (equivalent to 1.5 mg of curcumin). The dialysis membrane was then immersed in the beaker which containing 70 ml of dissolution medium (Acetate buffer pH 4.5+PEG 40%). During the experiment, the temperature of the dissolution medium was maintained at 37 °C under continuous stirring at 200 rpm using a magnetic stirrer (RCT-B-S022, IKA, India). At different time intervals, 3 ml of dissolution medium is withdrawn and replaced by the same volume of the fresh medium to maintain the sink conditions. The samples were further diluted and the amount of curcumin released from LPHNPs was quantified spectrophotometrically at 439 nm using UV-Visible Spectrophotometer (UV 1800, Shimadzu, Japan) with respect to blank [31, 32].

***In vitro* drug release kinetics**

To interpret the mechanism and kinetics of curcumin release from LPHNPs, the *in vitro* drug release data were fitted into different kinetic models like zero-order (cumulative amount of drug released vs. time), first-order (log cumulative percentage of drug remaining vs. time), Higuchi (cumulative percentage drug release vs. square root of time) and Korsmeyer-Peppas (log cumulative percentage drug release vs. log time) model. By comparing the obtained R^2 values of the above described model, the best-fit model was selected [33].

Stability studies

The stability studies of curcumin-loaded LPHNPs were performed as per ICH guidelines for a duration of 3 mo at two different storage conditions viz. normal conditions (25±2 °C and 75±5% RH) and refrigerated conditions (4±2 °C and 75±5% RH). During the period of the entire 3 mo, the curcumin-loaded LPHNPs were analyzed for changes in their particle size, polydispersity index and drug entrapment efficiency at a definite interval of 0, 30, 45, 60 and 90 d to assess the stability of the formulations [34].

Preparation of hydrogels containing LPHNPs

For the preparation of topical hydrogels, curcumin-loaded LPHNPs were incorporated into Carbopol 940 gel. Accurately weighed of Carbopol 940 polymer was dispersed in a sufficient quantity of distilled water and stirred continuously using a magnetic stirrer (RCT-B-S022, IKA, India) to form a gel-like mass. Now the prepared curcumin-loaded LPHNPs were added to the hydrogels and mixed properly under constant stirring at 1000 rpm for 5 min. The pH of the hydrogels was adjusted to ~6 by dropwise addition of triethanolamine solution and subsequently, other ingredients like methylparaben and glycerin were added to it that act as a preservative as well as a humectant. The prepared LPHNPs-loaded hydrogels (NLHG-1) were further allowed to stand overnight to remove entrapped air. Similarly, blank hydrogels (BHG-1) were prepared without the addition of LPHNPs using the same procedure [35, 36].

Characterization of hydrogel formulations

Physical appearance

The physical appearance of the prepared hydrogels was checked visually using a light microscope (Primo Star, ZEISS, Germany) for consistency, color, homogeneity and texture [37].

pH measurement

The pH of the prepared hydrogels were determined using a digital pH meter (pHTestr 10, Eutech Instruments, Singapore) at room temperature. Simply, 2 g of hydrogels were dispersed in 10 ml of distilled water and the electrode of the pH meter was then dipped into hydrogel dispersion and reading was noted [38].

Spreadability measurement

The spreadability of the prepared hydrogels were determined by measuring the spreading diameter of gel between two horizontal glass plates (20×20cm). Briefly, 1 g of the prepared hydrogels were placed in the mid of two glass plates and then a 200 g weight was applied on the upper glass plate for 5 min to spread the hydrogels. The diameters of the spreaded hydrogels were noted and then the top plate was pulled with the help of a string. Time is taken in which the upper glass plate separated from the lower glass plate was considered as a measure of spreadability. The spreadability was then determined according to the following formula [39]:

$$S = \frac{M.L}{T}$$

Where, S=spreadability, M=weight placed to the upper glass plate, L=length of the glass plate and T=time taken to separate the glass plates completely from each other.

Drug content estimation

To determine the drug content, 1 g of the prepared NLHG-1 hydrogels were dissolved in 25 ml of ethanol in a 100 ml volumetric flask. The volumetric flask was shaken for 2 h in order to get complete solubility of the drug and made up the volume 100 ml with ethanol. Then the solution was filtered using the Whatman syringe filter and after subsequent dilution, curcumin content in the filtrate was analyzed spectrophotometrically at 426 nm using UV-Visible Spectrophotometer (UV 1800, Shimadzu, Japan) with respect to blank ethanol [40].

***In vitro* skin permeation studies**

The full-thickness of pig ear skin was used for the skin permeation experiments. Fresh pig ears were collected from a local slaughterhouse of the Dibrugarh University Market. Initially, pig ears were thoroughly washed in running tap water and the hair on the skin surface was removed using an electric trimmer (NHT 1065, NOVA, India). The subcutaneous fat and other extraneous tissue adhering to the dermis were completely removed by using scissors and then it was kept in 2M sodium bromide solution for 36 h. After that, a full-thickness of skin was taken out and the fat adhering to the dermis and cut into appropriate sizes. Finally, the skin was rinsed with distilled water and was kept in 0.9% sodium chloride solution containing 1% formalin in a refrigerator (033E, Samsung, South Korea) at a temperature of-20 °C for further use.

The *in vitro* skin permeation through excised pig ear skin was performed by Franz diffusion cell. Briefly, the skin was clamped between the donor and the receptor chamber of a modified Franz diffusion cell (effective diffusion area of 1.77 cm^2) with a stratum corneum facing the donor compartment. The receptor chamber was then filled with dissolution medium (Acetate buffer pH 4.5 + 40% v/v PEG 400) and the temperature of the diffusion cell was maintained at 37 °C using a re-circulating water bath. The whole setup was placed over a magnetic stirrer (RCT-B-S022, IKA, India) with constant stirring at 150 rpm. After that, 1 g of prepared NLHG-1 hydrogels were gently placed in the donor chamber. At different time intervals, 2 ml of dissolution medium is withdrawn from the receptor chamber and replaced by the same volume of the fresh medium to maintain the sink conditions. The samples were further diluted and the amount of curcumin permeated from the NLHG-1 hydrogels were quantified spectrophotometrically at 439 nm using UV-Visible Spectrophotometer (UV 1800, Shimadzu, Japan) with respect to blank [41].

The permeation profile of curcumin through excised pig ear skin was determined by plotting the amount of drug permeated per unit area of skin (μg/cm^2) vs time. The steady-state flux (*Jss*) of curcumin was calculated from the slope of the plot using linear regression analysis and the permeability coefficient (Kp) of the drug through excised pig ear skin was calculated according to the following formula [42].

$$Kp = \frac{Jss}{C}$$

Where C= initial concentration of the drug in the donor compartment.

At the end of the skin permeation study, the mounted skin was removed from the compartments of the modified Franz diffusion cell and washed thoroughly with distilled water. The skin was then cut into small pieces and put into a stoppered conical flask containing 10 ml of ethanol and stirred continuously at 200 rpm using a magnetic stirrer (RCT-B-S022, IKA, India) for 24 h. After that, skin samples were homogenized by using a homogenizer (Ultra-Turrax T 25 Digital, IKA, India) and then centrifuged at 10000 rpm for 15 min to get the clear supernatant. The supernatant was then diluted with ethanol and the amount of curcumin retained in the skin was quantified spectrophotometrically at 426 nm using UV-Visible Spectrophotometer (UV 1800, Shimadzu, Japan) with respect to blank ethanol [43].

Skin accumulation of LPHNPs by TEM analysis

After the *in vitro* permeation study, the skin samples were successively collected for TEM analysis. Skin samples were washed properly and fixed for 3 h in a solution of 2.5% glutaraldehyde in 0.1M sodium cacodylate buffer (pH 7.2). The fixed samples were washed with 0.1 M sodium cacodylate buffer (pH 7.2) twice for 5 min and then post-fixed for 1 h at 4 °C with 1% osmium tetroxide solution. Post-fixed samples were dehydrated with ethanol and then embedded in epoxy resin. The resin embedding samples were placed in a desiccator for 30 min to remove any moisture content and finally observed under the transmission electron microscope (JEM 2100, JEOL, USA) operating at an accelerating voltage of 200 kV and photographs were captured in several different magnifications [44].

***In vivo* antipsoriatic efficacy**

The *in vivo* antipsoriatic efficacy of the prepared hydrogels were performed using healthy Wister Albino Rats of both sex and weighing of 150-200 g. All the rats were randomly divided into four groups, each containing three rats. Group I was taken as the positive control group (without any infection or treatment), Group II was taken as the negative control group (IMQ application and no treatment), Group III was taken as the standard group (IMQ application and treated with the standard marketed formulation of Betamethasone Valerate 0.1% w/w cream, GSK Pharmaceuticals Ltd., India) and Group IV was taken as the test group (IMQ application and treated with prepared NLHG-1 hydrogels). Before the experiment, animals were housed properly in polypropylene cages placed in a temperature-controlled environment at 22±3 °C under 12 h light and 12 h dark cycle with free access to food and water. The experiment in these animals was performed in accordance with the protocol approved by the Institutional Animal Ethical Committee (IAEC), Dibrugarh University, Dibrugarh, Assam, India under Approval No. IAEC/DU/149, Dated. 12/06/2018.

The psoriatic animal model was developed by the topical application of 5% w/w Imiquimod (IMQ) cream (Glenmark Pharmaceuticals Ltd., India). Briefly, the dorsal skin of each rat was shaved by using an electric trimmer (NHT 1065, NOVA, India) and IMQ cream was applied topically to the shaved skin (2.5×2.5 cm^2skin area) at an interval of 24 h up to 5 d. The induced areas were visually examined for symptoms resembling psoriasis such as erythema, scaling, skin thickening, infiltration of inflammatory cells as well as hyper-and Para-keratosis. After the induction period, all the animals were

treated for three weeks with the standard marketed gels and prepared NLHG-1 hydrogels once in a day, except the positive and negative control group. All the animals were observed at least twice daily to check the therapeutic efficacy of prepared hydrogel against psoriasis. At the end of the study period, all the rats were sacrificed according to the ethical guidelines of Dibrugarh University, India and skin samples of treated areas were excised histopathological analysis [45, 46].

Histopathological studies

The skin of the sacrificed animals was then subjected to histopathological analysis for the confirmation of the treatment efficacy of nanoformulations. The skin samples were collected from all the respective groups of animals and were fixed in 10% formalin fixative for 24 h. Collected skin samples were then processed in a tissue processor to remove the formalin content, embedded in paraffin wax for fixing and vertical skin sections (4 µm) were taken using a microtome. After removing the traces of paraffin, skin sections were mounted on the glass slide and stained with hematoxylin and eosin (H and E). The mounted specimens were finally observed under the light microscope fitted with a camera (BX 40, Olympus, Japan) and photographs were captured [47].

Statistical analysis

All the experimental data are expressed as mean±SD (n=3) and analyzed using one-way ANOVA followed by Dunnett's post hoc tests by GraphPad Prism Version 7.0 statistical software. A value of $P \leq 0.05$ was considered statistically significant.

RESULTS AND DISCUSSION

Preparation and optimization of curcumin-loaded LPHNPs

The curcumin-loaded LPHNPs were successfully prepared by the emulsification solvent evaporation method. In this investigation, ethylcellulose was used as an innermost hydrophobic polymeric core which encapsulating the anticancer drug curcumin and stearic acid was used outermost lipid layer that provides the protective shell over the polymeric core (fig. 1). All the ingredients used in the preparation of lipid-polymer hybrid nanoparticles were reported as biocompatible, biodegradable and safe for clinical purpose [48, 49].

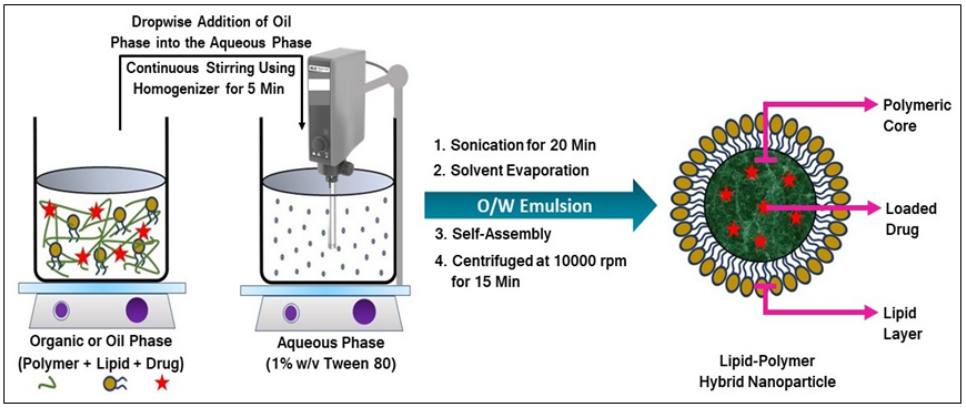

Fig. 1: Schematic representation of LPHNPs formulation process

For optimization purposes, the composition of the formulation was varied and several trials has been performed for the preparation of blank formulations. All the blank formulations were subjected to the characterization on the basis of particle size and polydispersity index to assess the effect of the lipid-to-polymer ratio. During optimization, it was found that ethylcellulose concentration lower than 20 mg rendered the structure of nanoparticles and also chances for low drug entrapment, whereas greater than 20 mg or excess amounts of polymer concentration produced larger size of nanoparticles, mainly due to formation of aggregation, which is further decrease the drug release and biostability of formulations [50]. Further, stearic acid concentration lower than 5 mg leading to sediment at the bottom of the container due to precipitation and coalescence of the polymeric core resulting from incomplete lipid layer coverage, whereas greater than 5 mg or excess amounts of lipid concentration resulting in the formation of thick lipid layers, which is further increasing the particle size as well as causing some challenges during drug release [51]. Hence, for the preparation of stable nanoformulations, the amount of ethylcellulose and stearic acid was fixed at 20 mg and 5 mg, respectively, as optimal and chosen for subsequent experiments with the addition of varying amounts of the drug. The composition of all the formulations is shown in table 1.

Table 1: Formulation design of blank and drug-loaded LPHNPs

Formulation code	Ethyl cellulose (mg)	Stearic acid (mg)	Drug (mg)	Ethanol (ml)	Tween 80 (% w/v)	Aqueous phase (ml)
BN-1	20	5	-	2	1	10
DLN-1	20	5	2	2	1	10
DLN-2	20	5	3	2	1	10
DLN-3	20	5	4	2	1	10

*BN: Blank LPHNPs, DLN: Drug-loaded LPHNPs.

Characterization of LPHNPs

Particle size, polydispersity index and zeta potential

The particle size, polydispersity index and zeta potential are the crucial parameters that describe the quality and stability of the formulations. All the developed formulations, both blank and drug-loaded LPHNPs were characterized for particle size, polydispersity index and zeta potential and the observed values are shown in table 2. The average particle size and polydispersity index of the prepared LPHNPs were measured by Dynamic Light Scattering using the particle size analyzer (90 Plus, Brookhaven Instrument, USA) and the zeta potential of the prepared LPHNPs were measured by Zetasizer (Nano ZS, Malvern Instruments, UK) (fig. 2). From the observation, it was found that particle size, polydispersity index and zeta potential were significantly affected by the concentration of polymer and lipid as well as the concentration of the drug. The

particle size and polydispersity index of DLN-1 to DLN-3 were increased with increment amount of the polymer and lipid. During the emulsification process, an increase in polymer and lipid concentration led to an increase in the viscosity of the organic phase leading to the formation of larger nanodroplets at the interface [52, 53]. The zeta potential measurement suggested that surface of the nanoparticles was negatively charged. This is mainly due to the presence of negatively charged stearic acid on the nanoparticle surface imparts anionic nature to the nanoparticles which confirmed that the polymeric core was successfully covered up by the lipid layer. The observed value revealed that drug-loaded LPHNPs were more stable than the blank since the zeta potential value of nanoparticles (>+30 mV or <-30 mV) were considered favorable for better colloidal stability of the developed nanoparticles [54].

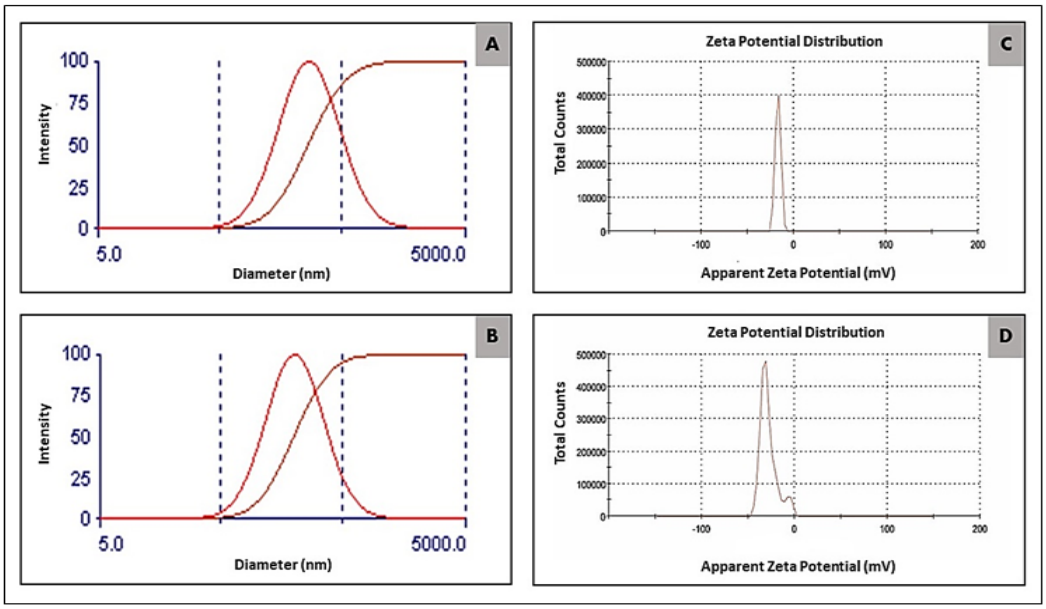

Fig. 2: Particle size distribution of (A) BN-1, (B) DLN-3 and Zeta potential of (C) BN-1, (D) DLN-3

Drug entrapment and drug loading efficiency

The drug entrapment and loading efficiency are two important parameters for assessing the total amount of drug feed during the formulation of nanoparticles. The drug entrapment and loading efficiency of all the LPHNPs formulations (DLN-1, DLN-2 and DLN-3) were determined using UV-Visible Spectrophotometer (UV 1800, Shimadzu, Japan) and the observed results are shown in table 2. From the observation, it was found that drug entrapment and loading efficiency were drastically decreased as the amount of polymer and lipid were increased. This is due to the fact that a higher amount of polymer and lipid would produce tinny size droplets with large surface areas, such that diffusion of the drug was very fast from the nanoparticles leading to the lower drug entrapment and loading efficiency [55].

Table 2: Characterization of LPHNPs

Formulation code	Particle size (nm)	Polydispersity index	Zeta potential (mV)	DEE (%)	DLE (%)
BN-1	190.8	0.379	-16.3	-	-
DLN-1	268.1	0.384	-36.7	81.83±0.23	2.37±0.14
DLN-2	300.1	0.373	-31.5	80.24±0.87	3.52±0.11
DLN-3	200.9	0.342	-28.3	87.40±0.99	4.57±0.04

*DEE: Drug entrapment efficiency, DLE: Drug loading efficiency., Data are presented as mean±SD (n=3).

Drug-excipient compatibility studies

For FT-IR analysis, the characteristic spectrums of the pure drug curcumin, ethylcellulose, stearic acid, physical mixture, blank LPHNPs (BN-1) and curcumin-loaded LPHNPs (DLN-3) were recorded and results are shown in fig. 3. From the FT-IR spectrum, it was observed that curcumin (fig. 3A) showed major characteristic peaks at 3475.58 cm^{-1} due to O-H stretching, 2909.05 cm^{-1}due to C-H stretching, 1625.9 cm^{-1} due to C=O stretching, 1499.73 cm^{-1}due to C-C stretching (aromatics) and 1263.27 cm^{-1} due to C-O stretching [56]. The FT-IR spectrum of ethyl cellulose (fig. 3B) indicates the characteristic bands at 3498.62 cm^{-1} due to O-H stretching, 2917.75 cm^{-1} due to C-H stretching, 1697.07 cm^{-1} due to C=O stretching and 1373.89 cm^{-1} due to C-H bending [57]. In the FT-IR spectrum of stearic acid (fig. 3C), a characteristics peak was observed at 2912.90 cm-1 due to O-H stretching, 2845.78 cm^{-1} due to C-H stretching, 1694.65 cm^{-1} due to C=O stretching and 1464.06 cm-1 due to C-H bending [58]. The spectrum of the physical mixture (fig. 3D) illustrates the characteristic bands of all the individual components without any remarkable shift from the normal position. The FT-IR spectrum of blank LPHNPs (fig. 3E) indicates the presence of distinct bands of both ethyl cellulose (1739.70 cm^{-1}) and stearic acid (2861.89 cm^{-1}), which further supports the development of formulation. However, in the spectrum of curcumin-loaded LPHNPs (fig. 3F), it was seen that curcumin reserved its identity, with a slight shift of distinct bands at 1453.91 cm^{-1} and 1252.80 cm^{-1}, suggesting C-C stretching and C-O stretching of the drug in the developed formulation, was not observed in the spectrum of blank LPHNPs which might be due to the overlapping of identical groups in ethyl cellulose and stearic acid [59].

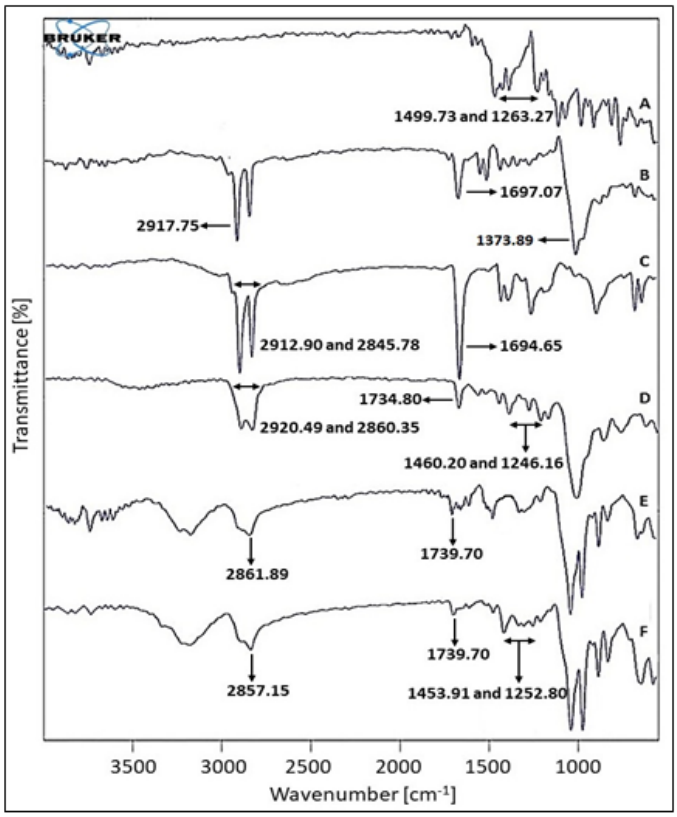

Fig. 3: FT-IR spectrums of (A) Curcumin, (B) Ethylcellulose, (C) Stearic acid, (D) Physical mixture, (E) Blank LPHNPs (BN-1), (F) Curcumin-loaded LPHNPs (DLN-3)

For DSC analysis, the thermograms of the pure drug curcumin, ethylcellulose, stearic acid, physical mixture, blank LPHNPs (BN-1) and curcumin-loaded LPHNPs (DLN-3) were recorded and results are shown in fig. 4. From the DSC thermogram, it was found that curcumin (fig. 4A) exhibits a sharp endothermic peak at 185.22 °C, indicating its melting point, respectively [60]. The thermogram of the ethylcellulose (fig. 4B) showed an exothermic peak at 187.74 °C, which is mainly due to the presence of crystalline domains within an amorphous base or semi-crystalline structure of the sample, whereas stearic acid (fig. 4C) as a lipid component of formulation showed an apparent endothermic peak at 62.28 °C [61, 62]. By comparing the DSC thermograms of the physical mixture (fig. 4D) and blank LPHNPs (fig. 4E) as well as curcumin-loaded LPHNPs (fig. 4F), it is clearly seen that both contain similar endothermic peaks. However, in the case of a physical mixture, the peaks are more prominent and sharper than the thermogram of formulations, which is mainly due to some components in the formulation may get covered or entrapped by other components. Further, the DSC thermogram of prepared curcumin-loaded LPHNPs showed the full disappearance of all the characteristics peaks of curcumin except those pertaining to ethylcellulose and/or stearic acid, confirms the molecular dispersion of the curcumin within the polymeric core of hybrid nanoparticles or existed in an amorphous form [63].

For XRD analysis, the diffractograms of the pure drug curcumin, ethylcellulose, stearic acid, physical mixture, blank LPHNPs (BN-1) and curcumin-loaded LPHNPs (DLN-3) were recorded and results are shown in fig. 5. From the XRD diffractograms, it was observed that the curcumin (fig. 5A) showed a group of sharp peaks in the range of 10-30 °, which reflecting its crystalline structure [64]. The XRD patterns of ethyl cellulose (fig. 5B) displayed a broad peak at 20.5°, indicating ethyl cellulose have mostly an amorphous region with semi-crystalline properties, whereas the diffractogram of stearic acid (fig. 5C) showed a typical diffraction peak at 21.0° and 24.0° indicating that stearic acid has good crystallization properties [65, 66]. The typical crystalline peaks of the curcumin (10°, 15°, 20.5°, 24° and 30°) are clearly visible in the physical mixture (fig. 5D), but these characteristics peaks are not apparent in the blank LPHNPs (fig. 5E) due to the absence of drug and curcumin-loaded LPHNPs (fig. 5F), which supports that curcumin was encapsulated in the polymeric core of the LPHNPs or might have undergone amorphization during formulation [67]. Therefore, drug excipient compatibility studies revealed that all the components used for the preparation of hybrid nanoparticles are compatible with each other, without producing any types of interactions.

Morphological studies

The outer shape and surface morphology of the prepared LPHNPs were assessed by SEM analysis and results are shown in fig. 6. The SEM photomicrographs of the blank (BN-1) (fig. 6A) and curcumin-loaded LPHNPs (DLN-3) (fig. 6B) affirmed that the shape of the nanoparticles was spherical and slightly pyritohedron with smooth surface characteristic and no such difference was observed in the morphological properties of nanoparticles due to the presence of the drug. Moreover, the SEM photomicrographs also revealed that the agglomeration of nanoparticles might be due to the lipidic nature of the nanoparticles surface and the drying process at the time of sample preparation prior to SEM analysis [68].

The internal structure and surface morphology of the prepared LPHNPs were further examined by TEM analysis and results are shown in fig. 6. TEM photographs of the blank (BN-1) (fig. 6C) and curcumin-loaded LPHNPs (DLN-3) (fig. 6D) suggested that the prepared nanoparticles were well identified with essentially spherical or round shape. As seen in TEM photographs, a relatively dense region was observed in the center portion. The probable reason is that during TEM analysis, the electrons are pass through the specimens like lipid or other materials, but in the case of a polymer, the electrons are unable to pass through the polymeric layer, as a result, the dense region was observed. This result indicates that the polymeric core was properly encapsulated within the lipid layers [69].

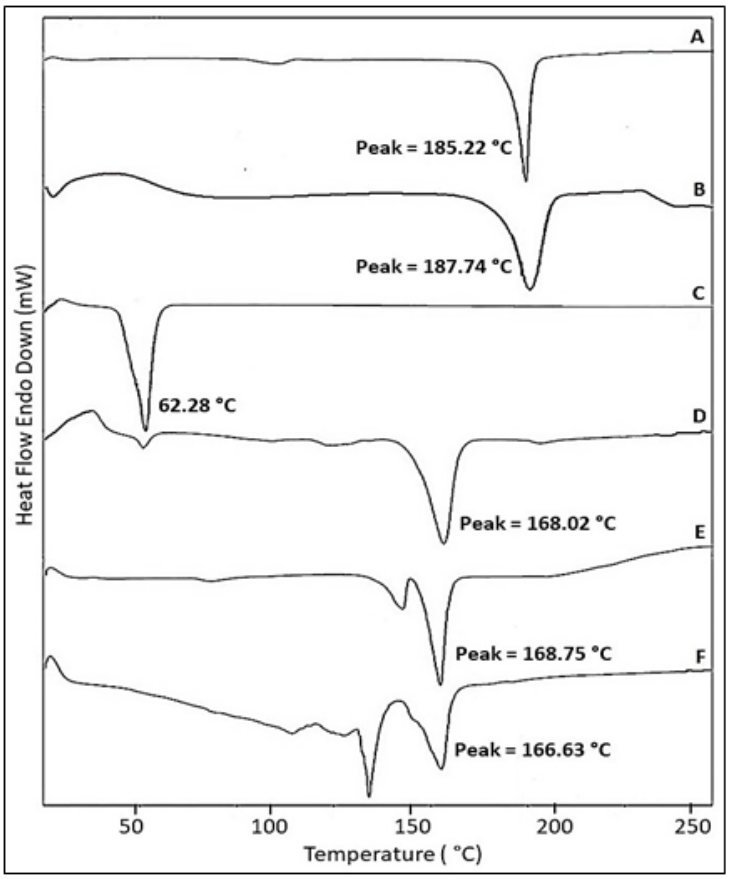

Fig. 4: DSC thermograms of (A) Curcumin, (B) Ethyl cellulose, (C) Stearic acid, (D) Physical mixture, (E) Blank LPHNPs (BN-1), (F) Curcumin-loaded LPHNPs (DLN-3)

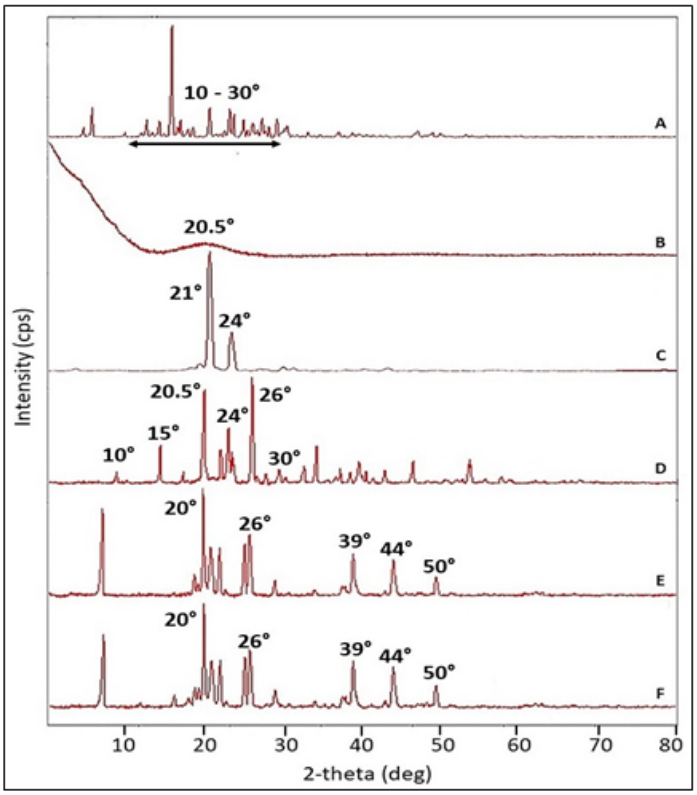

Fig. 5: X-ray diffractograms of (A) Curcumin, (B) Ethylcellulose, (C) Stearic acid, (D) Physical mixture, (E) Blank LPHNPs (BN-1), (F) Curcumin-loaded LPHNPs (DLN-3)

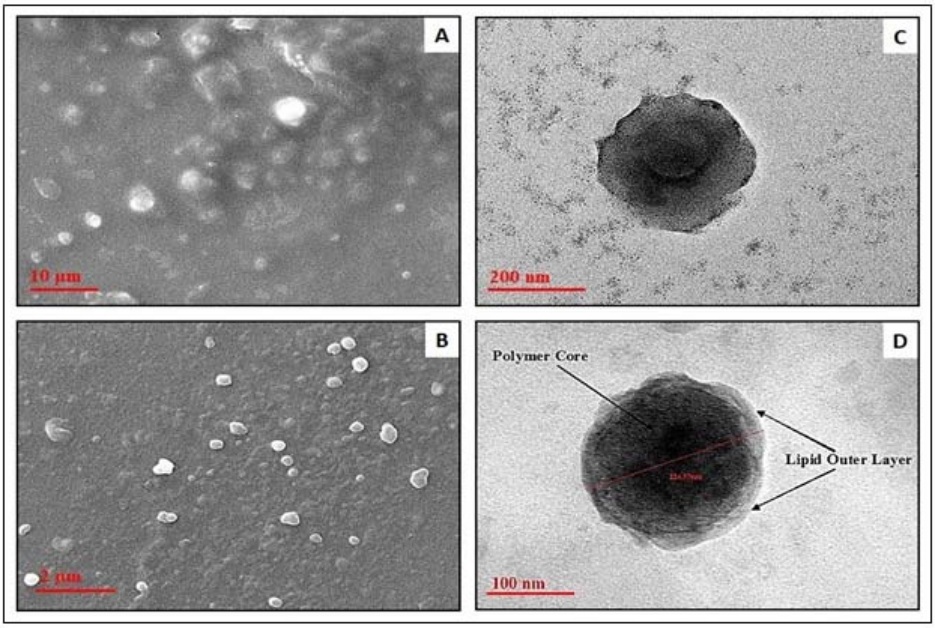

Fig. 6: Surface morphology: SEM images of (A) BN-1, (B) DLN-3 and TEM images of (C) BN-1, (D) DLN-3

In vitro drug release studies

The *in vitro* release studies of various curcumin-loaded LPHNPs formulations (DLN-1, DLN-2 and DLN-3) were performed using the dialysis bag method and the release profile of curcumin from the prepared LPHNPs are presented in fig. 7. During the experiment, 40% v/v PEG 400 was added to the phosphate buffer solution pH 4.5, to improve the water solubility of curcumin in maintaining sink condition throughout the drug release study. The drug release data revealed that all the formulations DLN-1, DLN-2 and DLN-3 were showed maximum drug release as 42.73±0.7, 46.16±1.4 and 55.37±1.4% up to 24 h, respectively. However, all the formulations DLN-1, DLN-2 and DLN-3 were showed an initial burst release of 32.60±1, 32.81±1.3 and 39.34±3.1% in 12 h period and thereafter showed slower sustained drug release. The reason behind the initial burst release is attributed that the presence of the drug on the surface of nanoparticles which might have got desorbed upon contact with the dissolution medium, while the slower and sustained release may be attributed to the diffusion of drug molecules through the polymer core matrix. This finding was further confirmed that successful incorporation of curcumin in the polymeric core of the LPHNPs could impactfully sustain the release of curcumin [70, 71].

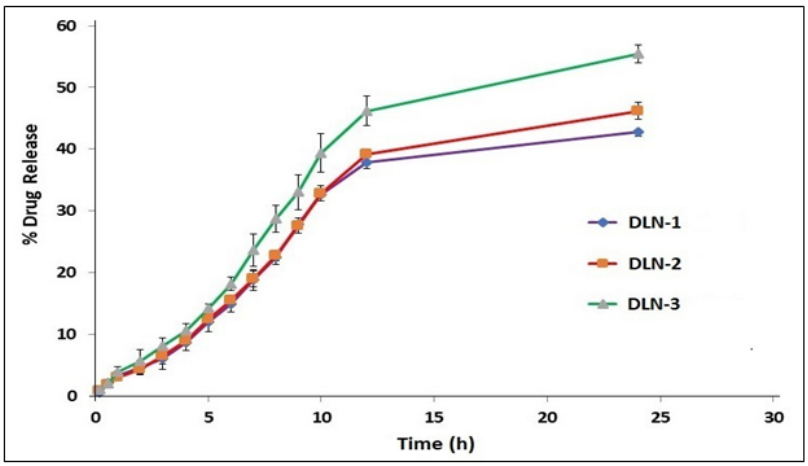

Fig. 7: *In vitro* drug release profile of prepared LPHNPs (DLN-1, DLN-2 and DLN-3) in acetate buffer pH 4.5+PEG 400 (40% v/v). Each data points are presented as mean±SD (n=3)

In vitro drug release kinetics

The drug release mechanism of all the curcumin-loaded LPHNPs formulations (DLN-1, DLN-2 and DLN-3) was interpreted by comparing the obtained correlational coefficient (R^2 value) of the various kinetic models like zero-order, first-order, Higuchi and Korsmeyer-Peppas model with one another by model fitting equation (table 3). A close observation of R^2 values of all the curcumin-loaded LPHNPs formulations (DLN-1, DLN-2 and DLN-3) attributed the release kinetic with the Korsmeyer-Peppas model with R^2 values of 0.975 (DLN-1), 0.973 (DLN-2) and 0.975 (DLN-3). The release exponent 'n' values are 0.91, 0.89 and 0.90 for DLN-1, DLN-2 and DLN-3, respectively, indicating that drug release from these formulations follows super case II transport mechanism operated by swelling and erosion of the polymer/lipid matrix in the dissolution medium [72, 73].

Table 3: Correlational coefficient (R^2) of different kinetic models for interpreting the drug release mechanism

Formulation code	Zero-order model		First-order model		Higuchi model		Korsmeyer-peppas model	
	R^2	K_0	R^2	K_1	R^2	K_H	R^2	n
DLN-1	0.855	2.075	0.880	-0.011	0.919	11.713	0.975	0.918
DLN-2	0.884	2.207	0.912	-0.012	0.919	11.713	0.973	0.897
DLN-3	0.884	2.644	0.923	-0.016	0.921	14.045	0.975	0.909

Stability studies

The stability of the prepared curcumin-loaded LPHNPs (DLN-1, DLN-2 and DLN-3) were investigated in terms of particle size, polydispersity index and drug entrapment efficiency (table 4). During the entire study period, it was observed that all the formulations were stable with minor variations in particle size and polydispersity index, without any significant changes in drug entrapment efficiency when stored at normal condition (25±2 °C) and refrigerated conditions (4±2 °C) for 90 d. The reason behind the slight variations in particle size and polydispersity index is that when stored at normal conditions the particle size and polydispersity index of the formulations were increased due to swelling, aggregation and photolytic degradation of particles. However, under refrigerated conditions, the particle size and polydispersity index were decreased due to the prevention of swelling, aggregation and photolytic degradation, stating better stability under these conditions. These results further suggested that temperature has a significant impact on LPHNPs properties and storage under refrigerated conditions is recommended for better stability [74, 75].

Preparation of hydrogels containing LPHNPs

After characterization of all the prepared curcumin-loaded LPHNPs (DLN-1, DLN-2 and DLN-3) in terms of particle size, polydispersity index, zeta potential, drug entrapment efficiency, drug loading efficiency and *in vitro* drug release profiles, the formulation DLN-3 with optimum physicochemical properties was selected for the preparation of topical hydrogels. The composition of the prepared topical hydrogels are shown in table 5.

Table 4: Stability studies of prepared curcumin-loaded LPHNPs (DLN-1, DLN-2 and DLN-3) for 90 d

Time (d)	Formulation code	Normal conditions (25±2 °C)			Refrigerated conditions (4±2 °C)		
		PS (nm)	PDI	DEE (%)	PS (nm)	PDI	DEE (%)
0	DLN-1	268.1	0.384	81.83±0.23	268.1	0.384	81.83±0.23
	DLN-2	300.1	0.373	80.24±0.87	300.1	0.373	80.24±0.87
	DLN-3	200.9	0.342	87.40±0.99	200.9	0.342	87.40±0.99
30	DLN-1	308.5	0.264	80.93±1.20	248.8	0.363	81.37±0.57
	DLN-2	342.5	0.403	80.24±1.30	297.1	0.375	80.40±1.20
	DLN-3	247	0.394	87.80±0.43	167.5	0.341	87.16±0.96
60	DLN-1	313.4	0.383	79.53±1.59	241.0	0.358	79.30±0.45
	DLN-2	352.2	0.366	82.18±0.74	287.9	0.307	80.51±0.69
	DLN-3	260.7	0.315	89.53±0.80	165.1	0.324	87.30±1.70
90	DLN-1	346.1	0.400	79.60±1.60	218.1	0.264	78.06±0.83
	DLN-2	368	0.388	81.78±0.78	282.2	0.357	79.88±2.14
	DLN-3	269.2	0.359	90.50±1.20	158.0	0.383	88.76±0.50

*PS: Particle size, PDI: Polydispersity index, DEE: Drug entrapment efficiency. Data are presented as mean±SD (n=3)

Table 5: Formulation design of blank and LPHNPs-loaded hydrogels

Gel formulation	Carbopol 940 (% w/v)	DLN-3 (% w/v)	Glycerin (% w/v)	Methyl paraben (% w/v)	Tri-ethanolamine	Distilled water
BHG-1	2	-	5	0.7	q. s.	q. s.
NLHG-1	2	0.1	5	0.7	q. s.	q. s.

*BHG: Blank hydrogels, NLHG: LPHNPs-loaded hydrogels.

Characterization of hydrogel formulations

The physicochemical properties like physical appearance, pH, spreadability and drug content of both blank and LPHNPs-loaded hydrogels were studied and results are shown in table 6.

Physical appearance

The physical appearance of prepared BHG-1 hydrogels was found to be off-white in color whereas, NLHG-1 hydrogels were found to be light yellow in color (fig. 8) due to the presence of curcumin with smooth in texture, semisolid consistency and highly homogenous nature [76].

pH measurement

The pH of the prepared BHG-1 and NLHG-1 hydrogels were found to be 4.90±0.15 and 5.53±0.32, respectively, which indicates that the pH of prepared hydrogels was slightly below 6.0 or almost near to the skin pH. It is physiologically suitable for topical use and also adequate for chemical stability since curcumin is unstable at pH 7.0 or above. As a result, skin irritation was avoided when topically applied on the skin surface [77].

Spreadability measurement

The spreadability of the prepared BHG-1 and NLHG-1 hydrogels were found to be 17.54±5.76 g-cm/sec and 20.94±14.52 g-cm/sec, respectively. These values suggest that the prepared hydrogels are easily spreadable on the skin surface by applying a small amount of shear. Moreover, the spreadability is not only exhibiting the behavior of the hydrogels but also provides better therapeutic efficacy, patient compliance as well as suitability for topical administration [78].

Table 6: Characteristics of blank and LPHNPs-loaded hydrogels

Gel formulation	Physical appearance	Homogeneity	pH	Spreadability (g-cm/sec)	Drug content (%)
BHG-1	Off white	Highly homogenous	4.90±0.15	17.54±5.76	-
NLHG-1	Light yellow	Highly homogenous	5.53±0.32	20.94±14.52	89.92±3.4

Data are presented as mean±SD (n=3).

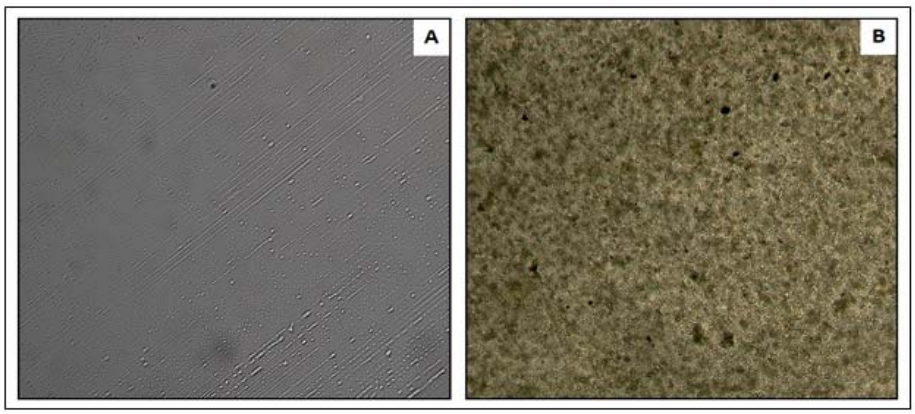

Fig. 8: Physical appearance of (A) BHG-1 hydrogels at 10X and (B) NLHG-1 hydrogels at 10X

Drug content estimation

The curcumin content in the prepared NLHG-1 hydrogels was found to be 89.92±3.4%, which indicates that drug-loaded LPHNPs were uniformly distributed and efficiently mixed in the hydrogels and the loss of drug or drug-loaded LPHNPs during formulation processes was minimal [79].

***In vitro* skin permeation studies**

The *in vitro* skin permeation study was performed using modified Franz diffusion cell and results suggested that prepared NLHG-1 hydrogels showed better permeation through the excised pig ear skin and retained in the skin layers for a prolonged period of time. As shown in fig. 9, the amount of curcumin permeated from the prepared NLHG-1 hydrogels was found to be sustained (38.39±2.67%) over a period of 12 h. Further, steady-state flux (*Jss*) and permeability coefficient (Kp) of the prepared NLHG-1 hydrogels were found to be 18.74±3.59 µg/cm^2/h and 1.87±0.36×10^{-2} cm/h, respectively, which indicates that the curcumin was significantly permeated through the pig ear skin from the NLHG-1 hydrogels. The enhanced skin permeation of the curcumin from the NLHG-1 hydrogels is mainly due to the smaller particle size and increased surface area of LPHNPs that interface with skin corneocytes and more effectively hydrated by the stratum corneum [80]. After investigating the skin permeation profile, the amount of curcumin retained in the skin was quantified spectrophotometrically and skin deposition of the curcumin in the NLHG-1 hydrogels was found to be 10.20±1.99 µg/ml, which indicated that the LPHNPs were strictly confined in the skin layers and exhibit maximum therapeutic efficacy in targeted localized skin area. This accumulation of curcumin in the epidermis might be attributed to that the uppermost layer of the epidermis i.e., stratum corneum consists of 70% proteins, 15% lipids and 15% water and this composition of the epidermis affirm retention of intact LPHNPs from which curcumin is released slowly in the epidermal site of skin where involving the hyper-proliferation of keratinocytes and psoriasis. Hence, observed results manifested that NLHG-1 hydrogels were suitable for further *in vivo* study [81, 82].

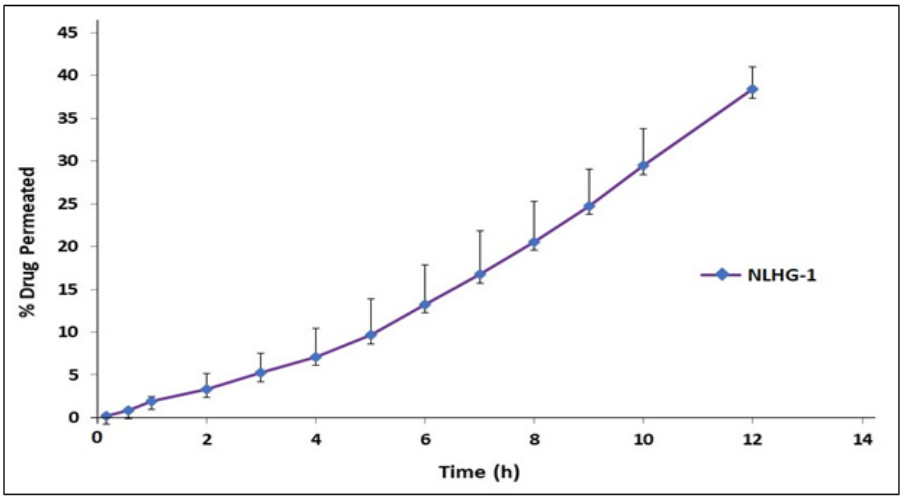

Fig. 9: *In vitro* drug permeation profile of prepared LPHNPs-loaded hydrogels (NLHG-1) employing pig ear skin. Each data points are presented as mean±SD (n=3)

Skin accumulation of LPHNPs by TEM analysis

To further confirm the skin accumulation of LPHNPs, skin samples from the *in vitro* permeation study were subjected to TEM analysis and photographs are shown in fig. 10. TEM images clearly revealed shape-dependent accumulation of various-shaped LPHNPs in the diverse layers of skin (red color dotted circles), indicates their penetration via the intercellular pathway. The number of LPHNPs observed inside epidermis, dermis and adipose tissues was dependent on particle size. As the particle size reduced, the higher amount of LPHNPs was found to aggregate in the deeper skin layers and eventually could reach the viable dermis. Earlier, Tak YK *et al.* (2015) studied skin penetration of silver nanoparticles (AgNPs) through mouse skin and found that AgNPs were permeated via an intercellular pathway in a size-dependent manner. In our study, LPHNPs accumulation appears to be in a similar way [83].

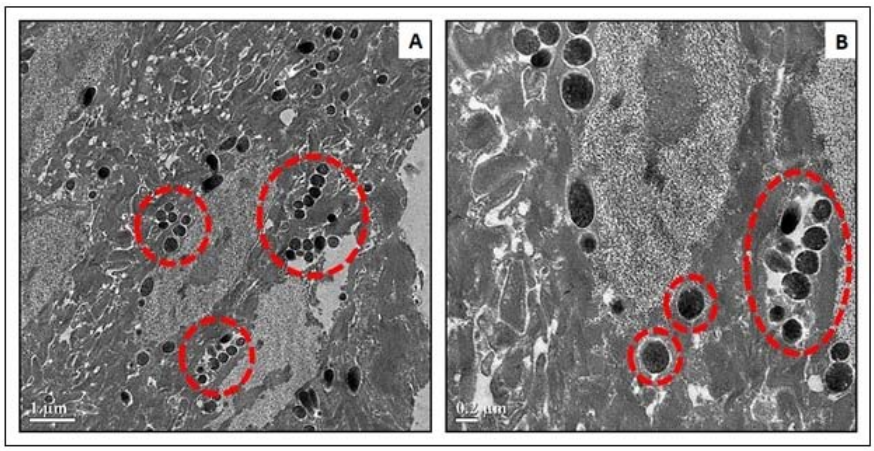

Fig. 10: TEM images of skin samples from *in vitro* skin permeation study

In vivo antipsoriatic efficacy

The *in vivo* antipsoriatic efficacy of the prepared NLHG-1 hydrogels and standard marketed gels were evaluated in healthy Wister albino rats using 5% w/w IMQ cream-induced psoriatic animal model (fig. 11). IMQ is an immune modulator mainly used for the treatment of external anogenital warts caused by human papillomaviruses (HPV). The topical application of IMQ on wild-type mice back skin was reported to induce skin lesions or inflammation that closely resembles to human psoriasis [84, 85]. After the induction period, the formation of lesions and inflammation over the rats skin were examined visually. Initially, all the animals and Group I animals (fig. 11A) showed normal skin structure without producing any clinical features of psoriasis-like inflammation, but the IMQ-treated rats back skin (Group II) (fig. 11B) started to exhibit symptoms of very mild thickening, erythema, swelling and scaling between 2-5 d. From day 6 onward, the inflammation was noticeable and got gradually increased in severity up to day 9 (fig. 11C and fig. 11D). These symptoms significantly reduced after topical application (started from day 10) of standard marketed gels in Groups III (fig. 11C') and prepared NLHG-1 hydrogels in Group IV (fig. 11D') for the period of three weeks. The results of the visual observation were further indicated that the rats were treated with prepared NLHG-1 hydrogels showed a maximum reduction of skin lesions, erythema, thickening and inflammation as compared to the standard marketed gels, which may be due to better skin penetration and accumulation of LPHNPs at the site psoriatic skin as well as the sustained release of curcumin for a long duration by the LPHNPs. Hence, the therapeutic potency of the prepared NLHG-1 hydrogels was found to be a magnificent and promising alternative formulation for psoriasis treatment [86-88].

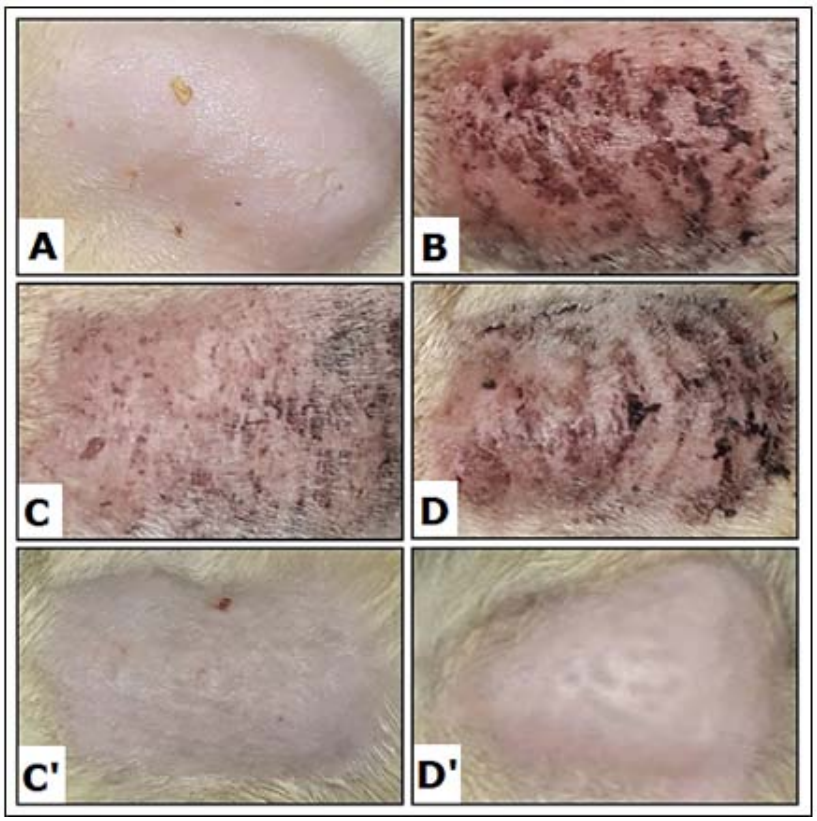

Fig. 11: *In vivo* evaluation of IMQ induced psoriatic skin (A) Positive control group, (B) Negative control group, (C/C′) Standard group, where C is the psoriatic skin and C′ is the cured skin, (D/D′) Test group, where D is the psoriatic skin and D′ is the cured skin

Histopathological studies

Histopathological analysis of the skin samples collected from a various group of animals i.e., positive control (Group I), negative control (Group II), standard (Group III) and test (Group IV) were done to observe the psoriatic features and the efficacy of treatment in the recovery of psoriatic skin to normal condition. The H and E stained images of collected skin samples from various groups of animals are shown in fig. 12.

In the positive control group (fig. 12A), no abnormal phenotype, dermal or epidermal irregularities were observed since this group does not treated with any chemicals. When compared to the positive control group, the negative control group (IMQ-treated group; fig. 12B) displayed inflammatory cell infiltration, irregular epidermal and subcutaneous tissue thickness due to hyperplasia of basal and suprabasal keratinocytes, suggesting the induction of psoriasis [89, 90]. The above-mentioned clinical features of psoriasis were significantly hindered after topical treatment with standard marketed gels (standard group; fig. 12C/C') and NLHG-1 hydrogels (test group; fig. 12D/D'). Both the standard marketed gels and NLHG-1 hydrogels treated group showed an almost similar therapeutic effect, but desirable outcomes were seen in the case of NLHG-1 hydrogels treated group, probably due to better skin penetration and accumulation of LPHNPs as well as the sustained release of curcumin for a prolonged period of time from the LPHNPs [91, 92].

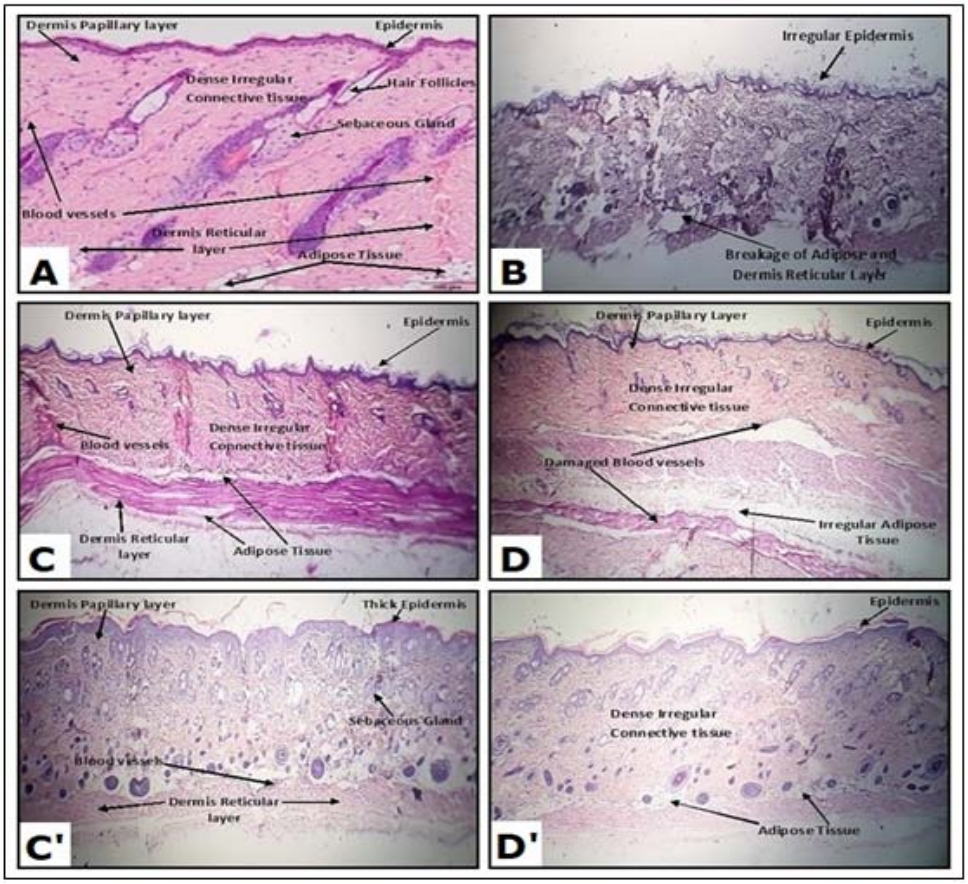

Fig. 12: Histopathological observation of rats skin via H and E staining (A) Positive control group, (B) Negative control group, (C/ C') Standard group, where C is the psoriatic skin and C' is the cured skin, (D/ D') Test group, where D is the psoriatic skin and D' is the cured skin

CONCLUSION

In the present study, LPHNPs-loaded hydrogels (NLHG-1) were developed and characterized for topical delivery of curcumin in the management of chronic inflammatory skin disorders related to psoriasis. The curcumin-loaded LPHNPs were successfully prepared by the emulsification solvent evaporation method and the results of *in vitro* characterization, drug-excipient compatibility and morphology of the developed LPHNPs were found to be in an appropriate range along with good compatibility and surface properties. *In vitro* drug release studies revealed that curcumin was released from the matrix of LPHNPs in a sustained manner over a period of 24 h via super case II transport mechanism followed by the Korsmeyer-Peppas model. Further, curcumin-loaded LPHNPs were incorporated into the hydrogel matrix for the topical administration of curcumin on IMQ-induced psoriatic skin. The results of *in vitro* skin permeation and skin retention study demonstrated that NLHG-1 hydrogels could significantly increase the permeation of curcumin and accumulation of LPHNPs into the pig ear skin for a prolonged period of time. Additionally, *in vivo* evaluation against IMQ-induced psoriasis in rats model and the histopathological study demonstrated that NLHG-1 hydrogels displayed better therapeutic efficacy as compared to the standard marketed gels by showing maximum reduction of skin lesions, erythema, thickening and skin inflammation. Therefore, it can be concluded that the prepared NLHG-1 hydrogels are a suitable and good alternative carrier for the management of various skin diseases like psoriasis.

ACKNOWLEDGEMENT

The authors are thankful to the Drug Delivery Research Laboratory (DDRL), Department of Pharmaceutical Sciences, Dibrugarh University, Dibrugarh, Assam, India, for providing the platform to conduct this work.

COMPLIANCE WITH ETHICAL STANDARDS

The Institutional Animal Ethical Committee (IAEC) of Dibrugarh University, Dibrugarh, Assam, India approved the experimental protocol (Approval No. IAEC/DU/149, Dated. 12/06/2018).

FUNDING

This work was financially supported by All India Council for Technical Education (AICTE)-PG Scholarship Scheme and Dibrugarh University Research Fellowship (DURF) Program.

AUTHORS CONTRIBUTIONS

All authors have contributed equally and approved the final version of the manuscript as submitted.

CONFLICT OF INTERESTS

The authors declare that they have no conflict of interest. All the tables and fig. are self-made and original.

REFERENCES

1. Parisi R, Symmons DP, Griffiths CE, Ashcroft DM. Identification and management of psoriasis and associated comorbidity (IMPACT) project team. Global epidemiology of psoriasis: a systematic review of incidence and prevalence. J Invest Dermatol 2013;133:377-85.
2. Alexis AF, Blackcloud P. Psoriasis in skin of color: epidemiology, genetics, clinical presentation, and treatment nuances. J Clin Aesthet Dermatol 2014;7:16-24.
3. Moorchung N, Khullar J, Mani N, Chatterjee M, Vasudevan B, Tripathi T. A study of various histopathological features and their relevance in the pathogenesis of psoriasis. Indian J Dermatol 2013;58:294-8.
4. Rendon A, Schäkel K. Psoriasis pathogenesis and treatment. Int J Mol Sci 2019;20:1475-502.
5. Zeng J, Luo S, Huang Y, Lu Q. Critical role of environmental factors in the pathogenesis of psoriasis. J Dermatol 2017;44:863-72.
6. Su YH, Fang JY. Drug delivery and formulations for the topical treatment of psoriasis. Expert Opin Drug Delivery 2008;5:235-49.
7. Wolf R, Orion E, Ruocco E, Ruocco V. Abnormal epidermal barrier in the pathogenesis of psoriasis. Clin Dermatol 2012;30:323-8.
8. Fereig SA, El-Zaafarany GM, Arafa MG, Abdel-Mottaleb MMA. Tackling the various classes of nano-therapeutics employed in topical therapy of psoriasis. Drug Delivery 2020;27:662-80.
9. Zhang Z, Tsai PC, Ramezanli T, Michniak Kohn BB. Polymeric nanoparticles-based topical delivery systems for the treatment of dermatological diseases. Wiley Interdiscip Rev Nanomed Nanobiotechnol 2013;5:205-18.
10. Hua S. Lipid-based nano-delivery systems for skin delivery of drugs and bioactives. Front Pharmacol 2015;6:1-5.
11. Niska K, Zielinska E, Radomski MW, Inkielewicz Stepniak I. Metal nanoparticles in dermatology and cosmetology: interactions with human skin cells. Chem Biol Interact 2018;1:38-51.
12. Zhang Y, Wu M, Wu M, Zhu J, Zhang X. Multifunctional carbon-based nanomaterials: applications in biomolecular imaging and therapy. ACS Omega 2018;3:9126-45.
13. Carter P, Narasimhan B, Wang Q. Biocompatible nanoparticles and vesicular systems in transdermal drug delivery for various skin diseases. Int J Pharm 2019;555:49-62.
14. Rahman M, Akhter S, Ahmad J, Ahmad MZ, Beg S, Ahmad FJ. Nanomedicine-based drug targeting for psoriasis: potentials and emerging trends in nanoscale pharmacotherapy. Expert Opin Drug Delivery 2015;12:635-52.
15. Gupta S, Bansal R, Gupta S, Jindal N, Jindal A. Nanocarriers and nanoparticles for skin care and dermatological treatments. Indian Dermatol Online J 2013;4:267-72.
16. Tahir N, Madni A, Balasubramanian V, Rehman M, Correia A, Kashif PM, *et al.* Development and optimization of methotrexate-loaded lipid-polymer hybrid nanoparticles for controlled drug delivery applications. Int J Pharm 2017;533:156-68.
17. Zhang L, Chan JM, Gu FX, Rhee JW, Wang AZ, Radovic Moreno AF, *et al.* Self-assembled lipid-polymer hybrid nanoparticles: a robust drug delivery platform. ACS Nano 2008;2:1696-702.
18. Hadinoto K, Sundaresan A, Cheow WS. Lipid-polymer hybrid nanoparticles as a new generation therapeutic delivery platform: a review. Eur J Pharm Biopharm 2013;85:427-43.
19. Mbese Z, Khwaza V, Aderibigbe BA. Curcumin and its derivatives as potential therapeutic agents in prostate, colon and breast cancers. Molecules 2019;24:4386-409.
20. Kamel AE, Fadel M, Louis D. Curcumin-loaded nanostructured lipid carriers prepared using Peceol™ and olive oil in photodynamic therapy: development and application in breast cancer cell line. Int J Nanomed 2019;14:5073-85.
21. Kotagale NR, Charde PB, Helonde A, Gupta KR, Umekar MJ, Raut NS. Studies on bioavailability enhancement of curcumin. Int J Pharm Pharm Sci 2020;12:20-5.
22. Gajra B, Dalwadi C, Patel R. Formulation and optimization of itraconazole polymeric lipid hybrid nanoparticles (Lipomer) using box behnken design. Daru 2015;23:3-17.
23. Bose RJ, Arai Y, Ahn JC, Park H, Lee SH. Influence of cationic lipid concentration on properties of lipid-polymer hybrid nanospheres for gene delivery. Int J Nanomed 2015;10:5367-82.
24. Massadeh S, Omer ME, Alterawi A, Ali R, Alanazi FH, Almutairi F, *et al.* Optimized polyethylene glycolylated polymer-lipid hybrid nanoparticles as a potential breast cancer treatment. Pharmaceutics 2020;12:666-79.
25. Jain A, Thakur K, Kush P, Jain UK. Docetaxel loaded chitosan nanoparticles: formulation, characterization and cytotoxicity studies. Int J Biol Macromol 2014;69:546-53.
26. Thadakapally R, Aafreen A, Aukunuru J, Habibuddin M, Jogala S. Preparation and characterization of PEG-albumin-curcumin nanoparticles intended to treat breast cancer. Indian J Pharm Sci 2016;78:65-72.
27. Govindaraju R, Karki R, Chandrashekarappa J, Santhanam M, Shankar A, Joshi HK, *et al.* Enhanced water dispersibility of curcumin encapsulated in alginate-polysorbate 80 nanoparticles and bioavailability in healthy human volunteers. Pharm Nanotechnol 2019;7:39-56.
28. Khan MA, Zafaryab M, Mehdi SH, Ahmad I, Rizvi MM. Characterization and anti-proliferative activity of curcumin loaded chitosan nanoparticles in cervical cancer. Int J Biol Macromol 2016;93:242-53.
29. Alizadeh N, Malakzadeh S. Antioxidant, antibacterial and anti-cancer activities of β-and γ-CDs/curcumin loaded in chitosan nanoparticles. Int J Biol Macromol 2020;147:778-91.
30. Anand P, Nair HB, Sung B, Kunnumakkara AB, Yadav VR, Tekmal RR, *et al.* Design of curcumin-loaded PLGA nanoparticles formulation with enhanced cellular uptake, and increased bioactivity *in vitro* and superior bioavailability *in vivo*. Biochem Pharmacol 2010;79:330-8.
31. Kumar SS, Mahesh A, Mahadevan S, Mandal AB. Synthesis and characterization of curcumin loaded polymer/lipid based nanoparticles and evaluation of their antitumor effects on MCF-7 cells. Biochim Biophys Acta 2014;1840:1913-22.
32. Behbahani ES, Ghaedi M, Abbaspour M, Rostamizadeh K. Optimization and characterization of ultrasound assisted preparation of curcumin-loaded solid lipid nanoparticles: application of central composite design, thermal analysis and X-ray diffraction techniques. Ultrason Sonochem 2017;38:271-80.
33. Dash S, Murthy PN, Nath LK, Chowdhury P. Kinetic modeling on drug release from controlled drug delivery systems. Acta Pol Pharm 2010;67:217-23.
34. Dave V, Sharma S, Yadav RB, Agarwal U. Herbal liposome for the topical delivery of ketoconazole for the effective treatment of seborrheic dermatitis. Appl Nanosci 2017;7:973-87.
35. Xu H, Wen Y, Chen S, Zhu L, Feng R, Song Z. Paclitaxel skin delivery by micelles-embedded Carbopol 940 hydrogel for local therapy of melanoma. Int J Pharm 2020;587:1-11.
36. Bhalekar MR, Pokharkar V, Madgulkar A, Patil N, Patil N. Preparation and evaluation of miconazole nitrate-loaded solid lipid nanoparticles for topical delivery. AAPS PharmSciTech 2009;10:289-96.
37. Dua K, Pabreja K, Ramana MV. Aceclofenac topical dosage forms: *in vitro* and *in vivo* characterization. Acta Pharm 2010;60:467-78.
38. El-Housiny S, Shams Eldeen MA, El-Attar YA, Salem HA, Attia D, Bendas ER, *et al.* Fluconazole-loaded solid lipid nanoparticles topical gel for treatment of pityriasis versicolor: formulation and clinical study. Drug Delivery 2018;25:78-90.

39. Rajan R, Vasudevan DT. Effect of permeation enhancers on the penetration mechanism of transfersomal gel of ketoconazole. J Adv Pharm Technol Res 2012;3:112-6.
40. Hosadurga RR, Rao SN, Jose J, Rompicharla NC, Shakil M, Shashidhara R. Evaluation of the efficacy of 2% curcumin gel in the treatment of experimental periodontitis. Pharmacogn Res 2014;6:326-33.
41. Shakeel F, Ramadan W, Ahmed MA. Investigation of true nanoemulsions for transdermal potential of indomethacin: characterization, rheological characteristics, and *ex vivo* skin permeation studies. J Drug Target 2009;17:435-41.
42. Patel D, Dasgupta S, Dey S, Ramani YR, Ray S, Mazumder B. Nanostructured lipid carriers (NLC) based gel for the topical delivery of aceclofenac: preparation, characterization, and *in vivo* evaluation. Sci Pharm 2012;80:749-64.
43. Ruela ALM, Figueiredo EC, Perissinato AG, Lima ACZ, Araujo MB, Pereira GR. *In vitro* evaluation of transdermal nicotine delivery systems commercially available in Brazil. Braz J Pharm Sci 2013;49:579-88.
44. Filon FL, Crosera M, Adami G, Bovenzi M, Rossi F, Maina G. Human skin penetration of gold nanoparticles through intact and damaged skin. Nanotoxicology 2011;5:493-501.
45. Sun L, Liu Z, Wang L, Cun D, Tong HHY, Yan R, *et al.* Enhanced topical penetration, system exposure and anti-psoriasis activity of two particle-sized, curcumin-loaded PLGA nanoparticles in hydrogel. J Controlled Release 2017;254:44-54.
46. Nimisha, Rizvi DA, Fatima Z, Neema, Kaur CD. Antipsoriatic and anti-inflammatory studies of *Berberis aristata* extract loaded nanovesicular gels. Pharmacogn Mag 2017;13(Suppl 3):S587-94.
47. Mangalathillam S, Rejinold NS, Nair A, Lakshmanan VK, Nair SV, Jayakumar R. Curcumin loaded chitin nanogels for skin cancer treatment via the transdermal route. Nanoscale 2012;4:239-50.
48. Maboos M, Yousuf RI, Shoaib MH, Nasiri I, Hussain T, Ahmed HF, *et al.* Effect of lipid and cellulose based matrix former on the release of highly soluble drug from extruded/spheronized, sintered and compacted pellets. Lipids Health Dis 2018;17:1-17.
49. Killen BU, Corrigan OI. Effect of soluble filler on drug release from stearic acid based compacts. Int J Pharm 2006;316:47-51.
50. Sharma N, Madan P, Lin S. Effect of process and formulation variables on the preparation of parenteral paclitaxel-loaded biodegradable polymeric nanoparticles: a co-surfactant study. Asian J Pharm Sci 2016;11:404-16.
51. Yuan Y, Chiba P, Cai T, Callaghan R, Bai L, Cole SPC, *et al.* Fabrication of psoralen-loaded lipid-polymer hybrid nanoparticles and their reversal effect on drug resistance of cancer cells. Oncol Rep 2018;40:1055-63.
52. Dave V, Yadav RB, Kushwaha K, Yadav S, Sharma S, Agrawal U. Lipid-polymer hybrid nanoparticles: development and statistical optimization of norfloxacin for topical drug delivery system. Bioact Mater 2017;2:269-80.
53. Sharma D, Maheshwari D, Philip G, Rana R, Bhatia S, Singh M, *et al.* Formulation and optimization of polymeric nanoparticles for intranasal delivery of lorazepam using box-behnken design: *in vitro* and *in vivo* evaluation. BioMed Res Int 2014;156010:1-14.
54. Lerata MS, D'Souza S, Sibuyi NRS, Dube A, Meyer M, Samaai T, *et al.* Encapsulation of variabilin in stearic acid solid lipid nanoparticles enhances its anticancer activity *in vitro*. Molecules 2020;25:830-41.
55. Mundargi RC, Shelke NB, Rokhade AP, Patil SA, Aminabhavi TM. Formulation and *in vitro* evaluation of novel starch-based tableted microsphere for controlled release of ampicillin. Carbohydr Polym 2008;71:42-53.
56. Rajan SS, Pandian A, Palaniappan T. Curcumin loaded in bovine serum albumin-chitosan derived nanoparticles for targeted drug delivery. Bull Mater Sci 2016;39:811-7.
57. Akbari Z, Amanlou M, Karimi Sabet J, Golestani A, Niasar MS. Characterization of carbamazepine-loaded solid lipid nanoparticles prepared by rapid expansion of supercritical solution. Trop J Pharm Res 2014;13:1955-61.
58. Wu X, Zhang L, Zhang X, Zhu Y, Wu Y, Li Y, *et al.* Ethyl cellulose nanodispersions as stabilizers for oil in water pickering emulsions. Sci Rep 2017;7:1-10.
59. Tahir N, Madni A, Correia A, Rehman M, Balasubramanian V, Khan MM, *et al.* Lipid-polymer hybrid nanoparticles for controlled delivery of hydrophilic and lipophilic doxorubicin for breast cancer therapy. Int J Nanomed 2019;14:4961-74.
60. Mathew MS, Vinod K, Jayaram PS, Jayasree RS, Joseph K. Improved bioavailability of curcumin in the gliadin-protected gold quantum cluster for targeted delivery. ACS Omega 2009;4:14169-78.
61. Davidovich Pinhas M, Barbut S Marangoni AG. Physical structure and thermal behavior of ethylcellulose. Cellulose 2014;21:3243-55.
62. Farboud ES, Nasrollahi SA, Tabbakhi Z. Novel formulation and evaluation of a Q10-loaded solid lipid nanoparticle cream: *in vitro* and *in vivo* studies. Int J Nanomed 2011;6:611-7.
63. Ishak RAH, Mostafa NM, Kamel AO. Stealth lipid polymer hybrid nanoparticles loaded with rutin for effective brain delivery-comparative study with the gold standard (Tween 80): optimization, characterization and biodistribution. Drug Delivery 2017;24:1874-90.
64. Wang W, Zhu R, Xie Q, Li A, Xiao Y, Li K, *et al.* Enhanced bioavailability and efficiency of curcumin for the treatment of asthma by its formulation in solid lipid nanoparticles. Int J Nanomed 2012;7:3667-77.
65. Mahnaj T, Ahmed SU, Plakogiannis FM. Characterization of ethyl cellulose polymer. Pharm Dev Technol 2013;18:982-9.
66. Wu B, Fu W, Kong B, Hu K, Zhou C, Lei J. Preparation and characterization of stearic acid/polyurethane composites as dual phase change material for thermal energy storage. J Therm Anal Calorim 2018;132:907-17.
67. Wang W, Chen T, Xu H, Ren B, Cheng X, Qi R, *et al.* Curcumin-loaded solid lipid nanoparticles enhanced anticancer efficiency in breast cancer. Molecules 2018;23:1578-90.
68. Mohan DC, Suresh A, Mukundan S, Gupta S, Viswanad V. Development and *in vitro* evaluation of nanolipid carriers of clobetasol propionate and pramoxine hydrochloride for topical delivery. Int J Appl Pharm 2018;10:28-36.
69. Tng DJ, Song P, Lin G, Soehartono AM, Yang G, Yang C, *et al.* Synthesis and characterization of multifunctional hybrid-polymeric nanoparticles for drug delivery and multimodal imaging of cancer. Int J Nanomed 2015;10:5771-86.
70. Jain A, Agarwal A, Majumder S, Lariya N, Khaya A, Agrawal H, *et al.* Mannosylated solid lipid nanoparticles as vectors for site-specific delivery of an anti-cancer drug. J Controlled Release 2010;148:359-67.
71. Wang W, Zhu R, Xie Q, Li A, Xiao Y, Li K, *et al.* Enhanced bioavailability and efficiency of curcumin for the treatment of asthma by its formulation in solid lipid nanoparticles. Int J Nanomed 2012;7:3667-77.
72. Das S, Das MK. Synthesis and characterization of thiolated jackfruit seed starch as a colonic drug delivery carrier. Int J Appl Pharm 2019;11:53-62.
73. Magesh B, Naidu PY, Rajarajeswar GR. S-adenosyl-l-methionine (SAMe)-loaded nanochitosan particles: synthesis, characterisation and in vitro drug release studies. J Exp Nanosci 2015;10:828-43.
74. Lakhani P, Patil A, Taskar P, Ashour E, Majumdar S. Curcumin-loaded nanostructured lipid carriers for ocular drug delivery: design optimization and characterization. J Drug Delivery Sci Technol 2018;47:159-66.
75. Thakkar HP, Patel BV, Thakkar SP. Development and characterization of nanosuspensions of olmesartan medoxomil for bioavailability enhancement. J Pharm Bioallied Sci 2011;3:426-34.
76. Vandana D, Pawar S. Formulation and evaluation of topical herbal gel containing inclusion complex of curcumin. Asian J Pharm Clin Res 2019;12:196-201.
77. Zamarioli CM, Martins RM, Carvalho EC, Freitas LAP. Nanoparticles containing curcuminoids (*Curcuma longa*): development of topical delivery formulation. Rev Bras Farmacogn 2015;25:53-60.
78. Zakaria AS, Afifi SA, Elkhodairy KA. Newly developed topical cefotaxime sodium hydrogels: antibacterial activity and *in vivo* evaluation. Biomed Res Int 2016;6525163:1-15.
79. Fong Yen W, Basri M, Ahmad M, Ismail M. Formulation and evaluation of galantamine gel as drug reservoir in transdermal patch delivery system. Sci World J 2015;495271:1-7.

80. Rajinikanth PS, Chellian J. Development and evaluation of nanostructured lipid carrier-based hydrogel for topical delivery of 5-fluorouracil. Int J Nanomed 2016;11:5067-77.
81. Rapalli VK, Kaul V, Waghule T, Gorantla S, Sharma S, Roy A, *et al.* Curcumin loaded nanostructured lipid carriers for enhanced skin retained topical delivery: optimization, scale-up, *in vitro* characterization and assessment of ex-vivo skin deposition. Eur J Pharm Sci 2020;152:1-55.
82. Kesharwani P, Jain A, Srivastava AK, Keshari MK. Systematic development and characterization of curcumin-loaded nanogel for topical application. Drug Dev Ind Pharm 2020;46:1443-57.
83. Tak YK, Pal S, Naoghare PK, Rangasamy S, Song JM. Shape-dependent skin penetration of silver nanoparticles: does it really matter? Sci Rep 2015;5:1-11.
84. Yuan J, Ni G, Wang T, Mounsey K, Cavezza S, Pan X, *et al.* Genital warts treatment: beyond imiquimod. Hum Vaccin Immunother 2018;14:1815-9.
85. Seifarth FG, Lax JE, Harvey J, DiCorleto PE, Husni ME, Chandrasekharan UM, *et al.* Topical heat shock protein 70 prevents imiquimod-induced psoriasis-like inflammation in mice. Cell Stress Chaperones 2018;23:1129-35.
86. Panonnummal R, Jayakumar R, Sabitha M. Comparative anti-psoriatic efficacy studies of clobetasol loaded chitin nanogel and marketed cream. Eur J Pharm Sci 2017;96:193-206.
87. Sathe P, Saka R, Kommineni N, Raza K, Khan W. Dithranol-loaded nanostructured lipid carrier-based gel ameliorate psoriasis in imiquimod-induced mice psoriatic plaque model. Drug Dev Ind Pharm 2020;45:826-38.
88. Walunj M, Doppalapudi S, Bulbake U, Khan W. Preparation, characterization and *in vivo* evaluation of cyclosporine cationic liposomes for the treatment of psoriasis. J Liposome Res 2020;30:68-79.
89. Moorchung N, Khullar J, Mani N, Chatterjee M, Vasudevan B, Tripathi T. A study of various histopathological features and their relevance in pathogenesis of psoriasis. Indian J Dermatol 2013;58:294-8.
90. Jia HY, Shi Y, Luo LF, Jiang G, Zhou Q, Xu SZ, *et al.* Asymmetric stem-cell division ensures sustained keratinocyte hyperproliferation in psoriatic skin lesions. Int J Mol Med 2016;37:359-68.
91. Avasatthi V, Pawar H, Dora CP, Bansod P, Gill MS, Suresh S. A novel nanogel formulation of methotrexate for topical treatment of psoriasis: optimization, *in vitro* and *in vivo* evaluation. Pharm Dev Technol 2016;21:554-62.
92. Khan MA, Pandit J, Sultana Y, Sultana S, Ali A, Aqil M, *et al.* Novel carbopol-based transfersomal gel of 5-fluorouracil for skin cancer treatment: *in vitro* characterization and *in vivo* study. Drug Delivery 2015;22:795-802.